Energy Conversion and Management 269 (2022) 116110

Contents lists available at ScienceDirect

Energy Conversion and Management

journal homepage: www.elsevier.com/locate/enconman

Thermodynamic assessment of a novel self-condensing sCO_2 recompression system with vortex tube

Tugberk Hakan Cetin, Jie Zhu *

Department of Architecture and Built Environment, University of Nottingham, University Park, Nottingham NG7 2RD, UK

ARTICLE INFO

Keywords:
Supercritical CO_2
Self-condensation
Vortex tube
Recompression cycle

ABSTRACT

Low temperature heat sink is required to condense the supercritical CO_2 (sCO_2) owing to its low critical temperature, this limits the sCO_2 power system application. In this paper, a self-condensing sCO_2 recompression system with vortex tube is proposed, which achieves the CO_2 condensation without the low temperature heat sink and recompression near the critical point in order to improve the system energy and exergy efficiencies. The system performance is investigated from the first and second laws of thermodynamics point of view, and parametric study is conducted to clarify the influences of key design and operation parameters, including the mass flow rate split ratio, the minimum and maximum pressures and temperatures. In a base case scenario with 100 kW power output, the system energy and exergy efficiencies reach 35.50 % and 58.21 % respectively. In the optimum operating condition, the system has the ability to provide 129.80 kW power output with the maximum energy efficiency of 41.90 % and exergy efficiency of 60.89 %.

1. Introduction

Over the last decades, electricity's share of the world's final energy consumption has increased gradually and reached 20 % currently. With electrification activities for net zero emission in 2050, it is projected that electricity will account for 50 % of the final energy use [1]. Thermal energy conversion cycles, such as concentrated solar power (CSP) and nuclear energy, will be the key contributors to achieving the net zero emission goal [2], the development of efficient and flexible thermal energy conversion technology is one of the promising solutions to meet the growing electricity demand.

Using CO_2 in the power generation system attracts many interests due to its characteristics, such as environmental friendliness, wide availability, safety, and thermal stability. The CO_2 low critical point (30.9 °C and 7.38 MPa) enables the utilization of its supercritical properties for power generation [3,4]. Compression near the CO_2 critical point not only allows for compact design in turbomachinery but also leads to low power consumption. The flexibility of direct and indirect CO_2 heating makes it applicable to the wide range of heat sources, such as the CSP [5], 4th generation nuclear power plant [6], coal fired power plant [7], and bottoming cycle for waste heat recovery with gas turbine [8].

There is intensive ongoing research on different supercritical CO_2 (sCO_2) configurations. Alfani et al. [8] carried out a optimization study by considering five different configurations including simple recuperative and recompressed recuperative cycle configurations. They found that simple recuperative cycle with a bypass loop is the optimum configuration with the maximum energy efficiency of 27.5 %. Li et al. [9] investigated design and off-design characteristics of a partial heating recuperative cycle, and conducted multi-objective optimization. They claimed that the cycle provides net power output of 8.67 MW with an exergy efficiency of 54.76 %. Chen et al. [10] also studied design and off-design performance of six different sCO_2 cycles powered by the CSP with thermal storage. They discovered that simple recuperative and recompression cycles are more suitable for highly varying weather conditions. Gao et al. [11] proposed a graph theory based configuration optimization framework and applied in the *meta*-configurations under the categories of no split, one split, and two splits in the cycle [12]. Their results show that with a 780 K heat source and a 295 K heat sink, energy efficiencies of these three categories reach up to 44.6 %, 48.1 % and 49.4 %, respectively. Due to the low critical temperature of CO_2, applicability of transcritical CO_2 Rankine cycle (TRC) is restricted by low temperature condenser that can condense CO_2 lower than 25 °C [13]. Angelino [14] designed partial and full condensation TRCs, and suggested that with the low temperature heat sinks, the condensation cycles have competitive efficiencies compared to the Rankine and Brayton cycles. Apart from the air and water, the refrigerant is also proposed to be used as the working

* Corresponding author.
E-mail address: jie.zhu@nottingham.ac.uk (J. Zhu).

https://doi.org/10.1016/j.enconman.2022.116110
Received 7 June 2022; Received in revised form 17 July 2022; Accepted 7 August 2022
Available online 13 August 2022

Nomenclature

COP	coefficient of performance
ex	specific exergy (kJ/kg)
Ėx	exergy (kW)
h	specific enthalpy(kJ/kg)
$\dot{m}$	mass flow rate (kg/s)
$\dot{Q}$	heat transfer rate (kW)
s	specific entropy(kJ/kg K)
S	entropy (kW/K)
sCO_2	supercritical Carbon Dioxide
SR	split ratio
P	Pressure (Mpa)
rpm	revolution per minute
T	temperature (°C or K)
TRC	transcritical

Greek Letters

Δ	difference
η_{II}	exergy efficiency
η_{en}	energy efficiency

Subscripts and indices

1,2,3..	states
ac	air cooler
comp	compressor
e	exit state
elec comp	electrical compressor
gen	generation
gh	gas heater
i	inlet state
irrev	irreversible
nozz	nozzle
turb	turbine

fluid in the TRC heat sink to solve condensation problem [15,16]. Yang et al. [17] integrated a LiBr/H_2O absorption refrigeration cycle into a transcritical CO_2 power system to tackle condensation problem, and found that the integrated system reaches energy efficiency of 7.50 %. Muhammed et al. [18] investigated a vapour compression integrated sCO_2 power cycle, and claimed that 10.67 % improvement in net power output is achieved by keeping the heat sink temperature at 50 °C. Luo et al. [19] also addressed the condensation issue by proposing a novel transcritical partial condensation system with recuperation, and found that the system energy efficiency is 27.41 % at the condensing temperature of 14.97 °C. Pan et al. [20,21] developed a self-condensing TRC concept by using an expansion valve to reduce pressure for solving condensation problem, and discovered that the maximum efficiency is 34.63 %. Ejector is also utilized for CO_2 self-condensation. Liu et al. [22] proposed a self-condensing TRC with an ejector refrigeration, and claimed that the system has the ability to produce 129.92 kW power and 254.96 kW cooling output simultaneously with an energy efficiency of 24.40 %. Similar self-condensation is achieved by vortex tube. Zhao et al. [23] used a vortex tube to replace the condenser in a compressed CO_2 energy storage system for independent operation, their system reaches 61.83 % exergy efficiency.

Using vortex tube as an expansion device in refrigeration system is getting lots of attention recently. Liu et al. [24] developed a transcritical CO_2 refrigeration cycle with vortex tube, and found that up to 10 % COP improvement can be achievable with vortex tube. Qyyum et al. [25] proposed a vortex tube integrated turbo-expander system for natural gas liquefaction, and claimed that using vortex tube for liquefaction reduces the system power consumption up to 68.5 %. Therewithal, application of vortex tube in power generation system also gains momentum in the literature. Cambronel et al. [26] proposed a sCO_2 Brayton cycle for waste heat recovery from the exhaust gas of internal combustion engine. They used a vortex tube to boost the upcoming exhaust gas and discovered that utilizing a vortex tube increases the cycle energy and exergy efficiencies of 1.85 % and 1.67 % respectively. Wang et al. [27] proposed a transcritical Rankine cycle with vortex tube, and claimed that the cycle exergy efficiency reaches 6.15 % when the turbine inlet temperature is 160 °C.

The above literature review shows that the supercritical and transcritical CO_2 condensation issues should be solved to achieve the high efficiency. Although the condensation can be achieved by a low temperature heat sink [28] or a expander [20], this paper presents a new concept to achieve the condensation without the heat sink and expander, that is self-condensation. A vortex tube is introduced in the recompression power cycle for self-condensation purposes. This novel vortex tube recompression takes place in the vicinity of critical point for compact size and high power output. Thus the advantages of both supercritical and transcritical CO_2 cycles are utilized. Thermodynamic analyses from the first and second law perspectives are carried out for the proposed design, parametric study is conducted in order to clarify effects of the minimum and maximum power block temperatures and pressures, and the mass flow rate split ratio on the system performance. Genetic algorithm is implemented for maximizing the system exergy efficiency. The output of this study provides the guides for the system design and optimization.

2. System description

The schematic diagram of the proposed self-condensing sCO_2 recompression system with vortex tube is given in Fig. 1, and the corresponding *T*-s diagram of the system is presented in Fig. 2. The system mainly consists of two blocks: power and vortex tube. The power block includes a gas heater, a turbine, a high temperature recuperator (HTR) and a low temperature recuperator (LTR), a cooler and the main compressor, the vortex tube block consist of a vortex tube, a pump and an electrical compressor. The high temperature and pressure stream from the gas heater (state 1) expands in the turbine and heats the upcoming streams from the HTR (states 18&19) and LTR (states 15&16). Subsequently, the stream from the LTR (state 4) mixes with the upcoming gas from the electrical compressor (state 14) and then is cooled in the cooler. Afterward, the stream from the cooler is split into two parts, one part (state 7) is diverted into the power block, i.e. main compressor to increase its pressure from near the critical pressure. The other part (state 8) is diverted into the vortex tube block, and it is further split into three portions in the vortex tube: saturated liquid (state 10), saturated vapour (state 11) and superheated vapour (state 12). The two vapour streams are mixed at first (state 13) and compressed (state 14) in the electrical compressor, then the high pressure stream mixes again with the upcoming stream from the LTR. As for the saturated liquid, it is pumped to reach the high pressure and heated in the LTR, then it is mixed with the stream from the main compressor (state 17) and heated again in the HTR, and further heated in the gas heater to reach high temperature and pressure to complete the cycle.

Main advantage of the system is achieving self-condensation in a vortex tube instead of a low temperature heat sink. By utilizing the vortex tube, the recompression takes place near the critical point to achieve a compact design and high performance.

3. Thermodynamic model

The system performance is investigated according to the first and

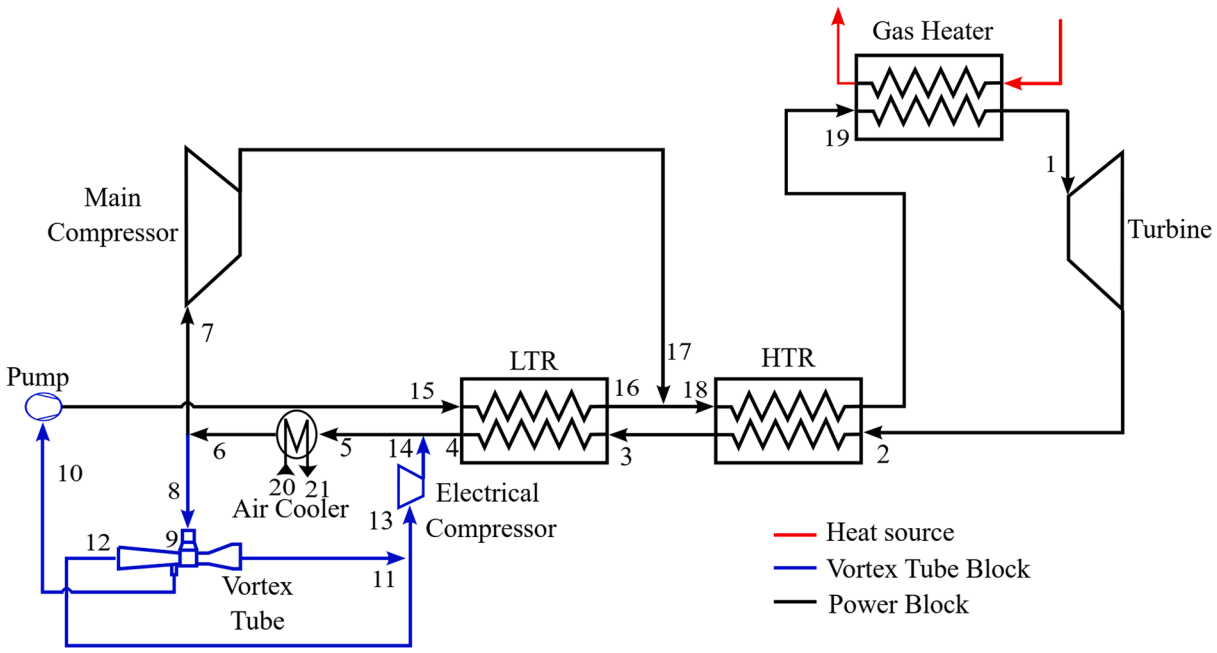

Fig. 1. Self-condensing sCO_2 recompression system with vortex tube.

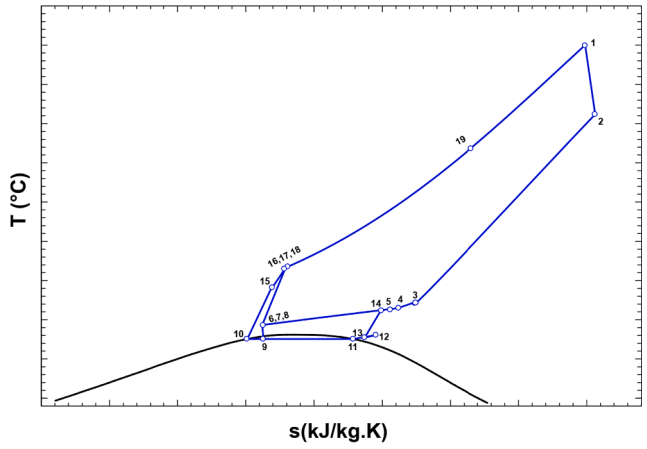

Fig. 2. *T*-s diagram of self-condensing sCO_2 recompression system with vortex tube.

second laws of thermodynamics, which give us both qualitative and quantitative information about system operating characters [29,30]. The following fundamental governing equations are employed in this study.

$$\sum \dot{m}_i = \sum \dot{m}_e \tag{1}$$

$$\sum \dot{Q} - \sum \dot{W} = \sum \dot{m}_e h_e - \sum \dot{m}_i h_i \tag{2}$$

$$\sum S_i - \sum S_e + S_{gen} = 0 \tag{3}$$

where $\dot{m}$ denotes the mass flow rate of the fluid, Q and W are the rates of heat input and power output respectively, h is the specific enthalpy and S_{gen} is the entropy generation within the system boundary associated with internal irreversibilities [29].

For the exergy assessment, the balance equation can be written as.

$$\sum \dot{E}x_Q - \dot{W} = \sum \dot{m}\, ex_e - \sum \dot{m}\, ex_i + I_{irrev} \tag{4}$$

$\dot{E}x$ is the exergy rate and I is the irreversibility rate. The exergy of heat transfer at temperature T can be expressed as [31]:

$$\dot{E}x_Q = \sum (1 - \frac{T_0}{T})\dot{Q} \tag{5}$$

The fluid specific exergy is.

$$ex = (h - h_0) - T_0(s - s_0) \tag{6}$$

where *0* subscript stands for the dead state of corresponding thermodynamic property.

The following assumptions are used to simplify the system mathematical models because the system has a complicated structure.

- The system operates under the steady state.
- Pressure drops in pipes and heat losses to the environment are neglected.
- The liquid and cold vapour leaving the vortex tube are at saturated states.
- The constant turbine, compressor and pump isentropic efficiencies are adopted.

3.1. Vortex tube model

The schematic of a vortex tube is shown in Fig. 3, it consists of a nozzle, a vortex chamber, a hot and a cold vapour exits and a liquid exit. The inlet high pressure working fluid expands in the nozzle, and then

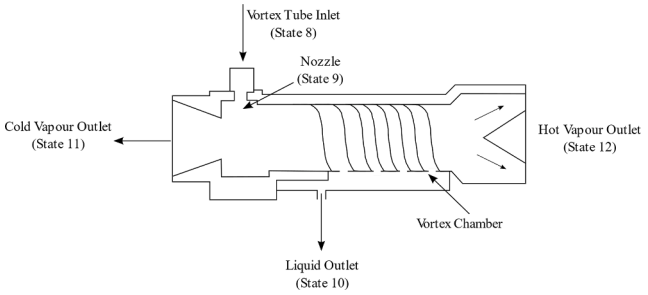

Fig. 3. Schematic diagram of the vortex tube.

tangentially flows in the vortex chamber where the flow velocity can reach 10^6 rpm [23]. The flow in the vortex tube is divided into two categories: peripheral and core flows. The peripheral flow increases its temperature gradually and leaves in hot end while the core flow leaves in the cold exit, which is called the Ranque–Hilsch effect [23,32]. When the fluid enters a two-phase region in the chamber, its condensate part is thrown to the tube wall due to the large centrifugal force. Thus, the inlet high pressure working fluid is divided into three portions: liquid (state 10), cold vapour (state 11) and hot vapour (state 12).

In this study, Mauer model [33] is utilized to achieve self-condensation of CO_2, which is suitable for the sCO_2 entering the vortex tube [32].

The enthalpy at the nozzle outlet can be calculated from:

$$h_9 = h_8 - \eta_{noz}(h_8 - h_{9,s}) \tag{7}$$

where η_{noz} is the isentropic efficiency of the nozzle.

Based on the nozzle outlet pressure, the quality of state 9 can be determined, and can be described as:

$$x_9 = x(h_9, P_9) \tag{8}$$

According to the state 9 quality, the liquid mass flow rate leaving the vortex tube can be calculated as:

$$\dot{m}_{10} = (1 - x_9)\dot{m}_9 \tag{9}$$

The cold mass fraction leaving the vortex tube is defined as:

$$y = \frac{\dot{m}_{11}}{\dot{m}_{11} + \dot{m}_{12}} \tag{10}$$

The mass balance for hot and cold vapours leaving the vortex tube is written as follows:

$$x_9\dot{m}_9 = \dot{m}_{11} + \dot{m}_{12} \tag{11}$$

Lastly, energy balance for the vortex tube is expressed as:

$$h_9 = (1 - x_9)h_{10} + x_9 y h_{11} + x_9(1 - y)h_{12} \tag{12}$$

3.2. Turbomachinery models

The compressor and pump isentropic efficiencies can be written as.

$$\eta_{comp/pump} = \frac{(h_{out,s} - h_{in})}{(h_{out} - h_{in})} \tag{13}$$

Specific compression work and power consumption for the main compressor are calculated as follows:

$$w_{comp} = SR(h_{17} - h_7) \tag{14}$$

$$\dot{W}_{comp} = \dot{m}_6 w_{comp} \tag{15}$$

where *SR* is the mass flow rate split ratio diverted to the main compressor. In order to simplify the mass balances and calculate specific work terms, all mass flow rates are normalized according to the total mass flow rate at the state 6. So, the *SR* can be expressed as:

$$SR = \frac{\dot{m}_7}{\dot{m}_6} \tag{16}$$

The remaining portion (*1-SR*) of the CO_2 is diverted to the vortex tube, and the liquid part is diverted to the pump. Specific work and power consumption of the pump can be calculated from:

$$w_{pump} = (1 - SR)(1 - x_9)(h_{15} - h_{10}) \tag{17}$$

$$\dot{W}_{pump} = \dot{m}_6 w_{pump} \tag{18}$$

The cold and hot vapours are mixed and then diverted to the electrical compressor. Specific work and power consumption of the electrical compressor can be written as:

$$w_{elc,comp} = (1 - SR)(x_9)(h_{14} - h_{13}) \tag{19}$$

$$\dot{W}_{elc,comp} = \dot{m}_6 w_{elc,comp} \tag{20}$$

The turbine isentropic efficiency can be calculated by:

$$\eta_{turb} = \frac{(h_{t,in} - h_{t,out})}{(h_{t,in} - h_{t,out,s})} \tag{21}$$

where subscript *t* denotes the turbine and *s* represents the isentropic process.

Power output of the turbine can be written as:

$$\dot{W}_{turb} = \dot{m}_1(h_1 - h_2) \tag{22}$$

Net power output of the system can be expressed as:

$$\dot{W}_{net} = \dot{W}_{turb} - \dot{W}_{comp} - \dot{W}_{elc,comp} - \dot{W}_{pump} \tag{23}$$

3.3. Heat exchanger model

In order to avoid the first and second law violations in heat exchanger, a comprehensive model is used. Each heat transfer equipment is divided into the specified number of segments, the minimum temperature differences, heat transfer rates and entropy generations of each segment are calculated.

Energy balances for the HTR and LTR are given in Eqs. (24) and (25) respectively.

$$(h_2 - h_3) = (h_{19} - h_{18}) \tag{24}$$

$$(h_3 - h_4) = (1 - SR)(1 - x_9)(h_{16} - h_{15}) \tag{25}$$

Heat input from the gas heater and heat removed from the air cooler can be expressed as:

$$\dot{Q}_{gh} = \dot{m}_1(h_1 - h_{19}) \tag{26}$$

$$\dot{Q}_{ac} = \dot{m}_5(h_5 - h_6) \tag{27}$$

where subscript *gh* represents the gas heater and *ac* stands for the air cooler.

3.4. Exergy analyses and performance indicators

Exergy analysis yields the important information about the system inefficiencies and tells us how much of the potential work is consumed by it [34]. Exergy balance of each component in the system is given in Table 1.

The system energy efficiency is defined as:

Table 1
Exergy balance for each component in the system.

Component	Exergy Balance
Turbine	$I_{turb} = \dot{E}x_1 - \dot{E}x_2 - \dot{W}_{turb}$
Hight Temperature Recuperator	$I_{htr} = (\dot{E}x_2 - \dot{E}x_3) + (\dot{E}x_{18} - \dot{E}x_{19})$
Low Temperature Recuperator	$I_{ltr} = (\dot{E}x_3 - \dot{E}x_4) + (\dot{E}x_{15} - \dot{E}x_{16})$
Air Cooler	$I_{ac} = (\dot{E}x_4 - \dot{E}x_5) + (\dot{E}x_{20} - \dot{E}x_{21})$
Main Compressor	$I_{mc} = \dot{E}x_7 + \dot{W}_{comp} - \dot{E}x_{17}$
Pump	$I_{pump} = \dot{E}x_{10} + \dot{W}_{pump} - \dot{E}x_{15}$
Vortex Tube	$I_{vt} = \dot{E}x_8 - \dot{E}x_{10} - \dot{E}x_{11} - \dot{E}x_{12}$
Electrical Compressor	$I_{elc,comp} = \dot{E}x_{13} + \dot{W}_{elc,comp} - \dot{E}x_{14}$
Mixing (before HTR)	$I_{mixing,htr} = \dot{E}x_{16} + \dot{E}x_{17} - \dot{E}x_{18}$
Mixing (before Air cooler)	$I_{mixing,ac} = \dot{E}x_{14} + \dot{E}x_4 - \dot{E}x_5$
Gas Heater	$I_{gh} = \dot{E}x_Q + \dot{E}x_{19} - \dot{E}x_1$

$$\eta_{en} = \frac{\dot{W}_{net}}{\dot{Q}_{gh}} \tag{28}$$

The system exergy efficiency also can be expressed as follows:

$$\eta_{II} = \frac{\dot{W}_{net}}{\dot{E}x_1 - \dot{E}x_{19}} \tag{29}$$

3.5. Optimization

Genetic algorithm is implemented in order to maximize the system performance. The genetic algorithm is nature inspired heuristic optimization method where objective function is evaluated throughout population and fitness of each individual, the individuals with the best fitness values generate offspring of new generations. Crossover and mutations are also introduced in each generation to kept population diverse, and the optimization is terminated when the set criteria are achieved [35,36].

In this study, the minimum and maximum power block pressures and temperatures, and split ratio are the variables. To account for both energetic and exergetic constraints, the system exergy efficiency is chosen as the objective function [37]. The formulated optimization problem and variable limitations are given below.

$$Max_x\{\eta_{II}\} \tag{30}$$

where $\times$ is the vector of

$$x = \{P_{min}, P_{max}, T_{max}, T_{min}, SR\} \tag{31}$$

Subject to

$$8MPa < P_{min} < 8.5MPa \tag{32}$$

$$16\,MPa < P_{max} < 20\,MPa \tag{33}$$

$$400^{\circ}\mathrm{C} < T_{max} < 800^{\circ}\mathrm{C} \tag{34}$$

$$31^{\circ}\mathrm{C} < T_{min} < 32.5^{\circ}\mathrm{C} \tag{35}$$

$$0.1 < SR < 0.7 \tag{36}$$

4. Calculation procedure and model validation

Comprehensive simulation model that accepts the system operation parameters, such as the minimum and maximum pressures and temperatures, minimum temperature difference (ΔT_{min}) in heat exchanger, split ratio and net power output, is created in MATLAB environment. For

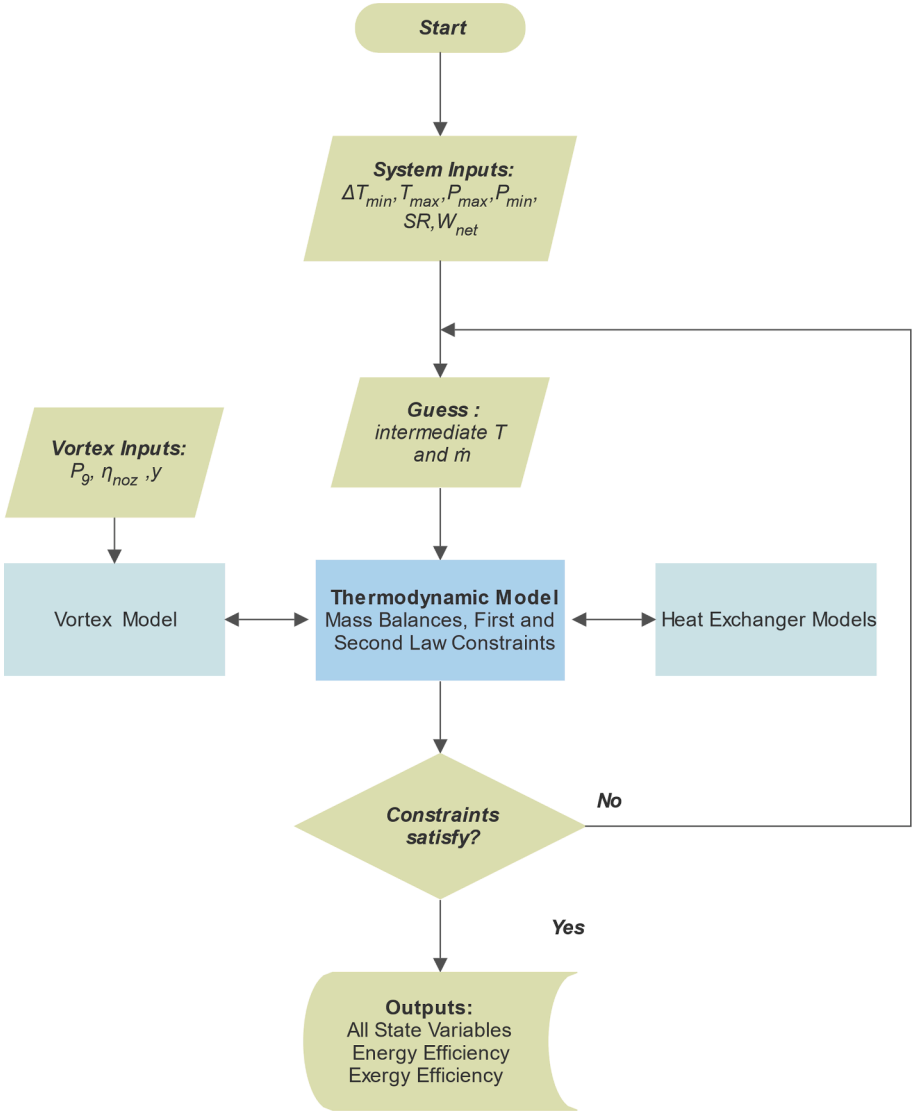

Fig. 4. Flowchart of calculation procedure for the proposed system.

thermodynamic properties of CO_2, open source thermophysical property package CoolProp is used [38].The extensive component models are generated for heat transfer equipment in order to ensure operation without violation of the first and second laws, and Mauer model [33] is utilized for the vortex tube. Iterative calculation procedure is carried out until the first and second law constraints are satisfied. The general calculation procedure is given in Fig. 4. For the optimization, the control parameters for genetic algorithm are specified as population size of 50, the maximum number of generations of 300 and crossover fraction of 0.8 [39].

In order to verify the developed turbomachinery and heat exchanger models, a stand-alone sCO_2 recuperative cycle is modelled and the simulation results are compared with those in the literature [40] as represented in Table 2. The highest data divergence between this study and the cited recuperative cycle is 2.78 % for the compressor specific work.

As for the vortex tube model, a transcritical vortex tube refrigeration cycle is modelled and the results are compared with the data presented in the literature [41]. The verification results under different vortex tube inlet temperatures are given in Table 3. The maximum performance deviation between the transcritical vortex tube refrigeration cycle and the literature is 0.21 %.

These comparisons demonstrate the accuracies of the developed models in this study; therefore, the developed models can be used to predict the system performance under various operating conditions.

5. Results and discussion

The performance of the proposed self-condensing sCO_2 recompression system is investigated in this section. Parametric analyses are conducted to explore the effects of key design and operating parameters, including the minimum power block temperature and pressure, maximum power block temperature and pressure, and the mass flow rate split ratio, on the system energy and exergy efficiencies.

5.1. Base case scenario performance

In the base case scenario, the net power output of 100 kW is targeted, while the turbine inlet temperature, minimum and maximum power block pressures and split ratio are set as 600 °C, 8Mpa, 20Mpa and 0.3 respectively. All parameters in the base case scenario are presented in Table 4.

The stream and performance data in the base case scenario are given in Tables 5 and 6. The turbine produces 124.64 kW power output while the main and electrical compressors, and pump consume 8.43 kW, 0.417 kW and 15.79 kW power respectively, so the system net power output is 100 kW to meet the target. The system energy and exergy efficiencies are 35.50 % and 58.21 % respectively.

For the sake of comparison, the performance of a traditional sCO_2 recuperation cycle is given in Table 6. Under the same operating conditions as given in Table 4 and the same net power of 100 kW, the energy and exergy efficiencies of the self-condensing recompression system are 35.50 % and 58.21 % respectively while the traditional sCO_2 recuperation system efficiencies are 34.88 % and 57.20 %. Although the turbine power output of traditional sCO_2 recuperation system is slightly higher than that of the proposed system, the power consumption in the traditional sCO_2 recuperation system is higher than that in the proposed system. As a result, the proposed self-condensing sCO2 recompression system has higher energy and exergy efficiencies.

Irreversibilities in the components and temperature distributions in the HTR, LTR and air cooler are given in Fig. 5, Fig. 6 a), b) and c), respectively. The highest irreversibility contributor is the HTR with a value of 45.12 kW, this is due to the high heat duty in the HTR. The followed large contributors are the gas heater, turbine and air cooler. Compared with the other heat transfer equipment, the LTR has lower irreversibility with a value of 0.1381 kW due to the low heat duty. The electrical compressor is the lowest contributor with a value of 0.079 kW

Table 2
Verification results for recuperative cycle.

Recuperative Cycle			
Parameter	**Reference [40]**	**Model**	**Absolute Difference**
Turbine specific work (kJ/kg)	125.87	124.6	1.01 %
Compressor specific work (kJ/kg)	20.88	20.3	2.78 %
Specific heat input (kJ/kg)	280.39	277.47	1.04 %
Energy Efficiency	0.3744	0.3758	0.37 %

Table 3
Verification results for vortex tube.

Transcritical Vortex Tube Refrigeration Cycle (cold vapour fraction: 0.5, Discharge Pressure: 9 MPa)			
Parameter	**COP**		**Absolute Difference**
Vortex Tube Inlet Temperature (°C)	**Reference [41]**	**Model**	
25	3.6804	3.6869	0.17 %
30	3.3143	3.3103	0.12 %
35	2.8223	2.8283	0.21 %

Table 4
Parameters used in this study [32,40,42].

Parameter	Value
Recuperator Minimum Temperature Difference ΔT_{min} (°C)	5
Maximum Power Block Pressure P_{max} (Mpa)	20
Minimum Power Block Pressure P_{min} (Mpa)	8.0
Maximum Power Block Temperature T_{max} (°C)	600
Minimum Power Block Temperature T_{min} (°C)	32.0
Vortex Tube Outlet Pressure (Mpa)	6.8
Turbine Isentropic Efficiency η_{turb} (%)	80
Main Compressor Isentropic Efficiency η_{comp} (%)	70
Electrical Compressor Isentropic Efficiency $\eta_{elc,comp}$ (%)	80
Pump Isentropic Efficiency η_{pump} (%)	80
Dead State Pressure (kPa)	101.325
Dead State Pressure (°C)	25

Table 5
Stream data for the self-condensing sCO_2 recompression system.

State	$\dot{m}$ *(kg/s)*	*P (Mpa)*	*T (°C)*	*h (kJ/kg)*	*s (kJ/kg.K)*	*ex (kJ/kg)*	$\dot{E}x$ *(kW)*
1	1.091	20	600.00	1097.39	2.81	568.39	620.24
2	1.091	8.0	498.61	983.17	2.85	442.96	483.37
3	1.091	8.0	63.43	464.55	1.85	223.48	243.87
4	1.091	8.0	58.76	455.70	1.82	222.53	242.83
5	1.163	8.0	57.28	452.73	1.81	222.23	258.38
6	1.163	8.0	32.00	296.42	1.31	215.21	250.21
7	0.349	8.0	32.00	296.42	1.31	215.21	75.06
8	0.814	8.0	32.00	296.42	1.31	215.21	175.15
9	0.814	6.8	27.41	294.92	1.31	213.33	173.62
10	0.742	6.8	27.41	286.32	1.29	213.26	158.33
11	0.036	6.8	27.41	384.37	1.61	214.05	7.64
12	0.036	6.8	33.57	418.66	1.72	214.60	7.66
13	0.071	6.8	29.52	401.52	1.67	214.24	15.30
14	0.071	8.0	40.96	407.37	1.67	218.98	15.64
15	0.742	20	53.12	307.59	1.30	231.61	171.96
16	0.742	20	58.43	320.60	1.33	232.83	172.86
17	0.349	20	58.43	320.60	1.33	232.83	81.21
18	1.091	20	58.43	320.60	1.33	232.83	254.07
19	1.091	20	390.76	839.22	2.48	410.95	448.44
20	36.05	0.2	25	424.20	3.68	58.16	2097.45
21	36.05	0.2	30	429.24	3.70	58.21	2098.96

Table 6
Performance results for the self-condensing sCO_2 recompression system and traditional recuperation sCO_2 system in base case scenario.

	Self-condensing sCO_2 Recompression system	Traditional sCO_2 Recuperation system
Parameter	**Value**	**Value**
$\dot{W}_{turb}$ (kW)	124.64	126.84
$\dot{W}_{comp}$ (kW)	8.43	26.84
w_{comp} (kJ/kg)	7.25	21.16
$\dot{W}_{elec,comp}$ (kW)	0.417	–
$w_{elec,comp}$ (kJ/kg)	0.358	–
$\dot{W}_{pump}$ (kW)	15.79	–
w_{pump}(kJ/kg)	13.58	–
$\dot{W}_{net}$ (kW)	100	100
Q_{gh} (kW)	281.72	286.69
η_{en} (%)	35.50	34.88
η_{II} (%)	58.21	57.20

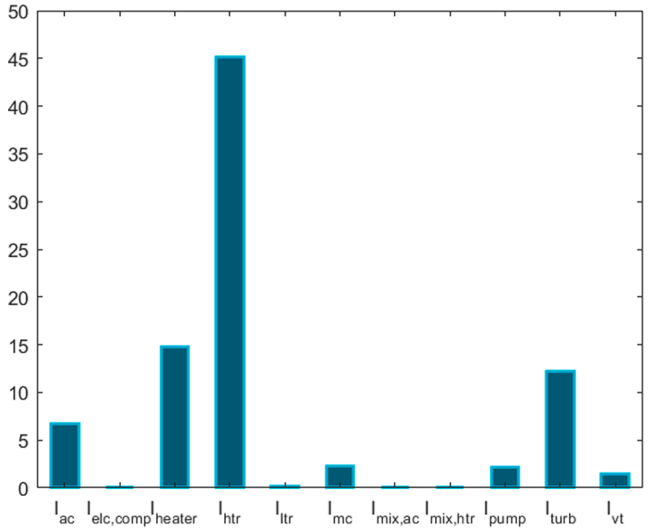

Fig. 5. Irreversibilities associated with each component.

owing to the relatively low mass flow rate and pressure ratio.

5.2. Parametric studies

Parametric studies are conducted to identify the effects of operation and design parameters on the system thermodynamic performance. All other parameters in the system are kept constant as stated in base case scenario except one indicated as the variable.

5.2.1. Effects of the minimum power block pressure

The variations of the turbine power production, compressor and pump consumption with the minimum power block pressure are shown in Fig. 7, correspondingly the system energy and exergy efficiencies are presented in Fig. 8. As the minimum pressure rises from 8.0Mpa to 8.5Mpa, the power consumption of main compressor decreases from 8.43 kW to 7.76 kW due to the reduction in its compression ratio, while the power consumption of the electrical compressor also decreases from 0.41 kW to 0.14 kW owing to both decreases in its mass flow rate and compression ratio. Due to those reasons, the system energy efficiency decreases from 35.50 % to 34.77 % and exergy efficiency reduces from 58.21 % to 56.77 %. The minimum pressure is also the vortex inlet pressure, so it influences the vortex tube performance as well. As the minimum pressure increases, more liquid working fluid is produced in the vortex tube, which is diverted to the turbine to increase the power output. But at the same time, the turbine pressure ratio is reduced to decrease the turbine power output. This trade off leads to the maximum turbine power output of 125.08 kW at the minimum pressure of 8.18 Mpa.

5.2.2. Effects of the maximum power block pressure

The variations of power production from the turbine and power consumption by main and electrical compressors and pump with the maximum power block pressure are shown in Fig. 9, the system energy and exergy efficiencies are given in Fig. 10. As the maximum pressure rises from 16Mpa to 20Mpa, the power output from the turbine increases from 95.89 kW to 124.64 kW due to high expansion ratio, while the power consumption by the pump and main compressor also increases from 5.73 kW and 11.21 kW to 8.43 kW and 15.79 kW respectively due to the high compression ratio. The electrical compressor is not affected by the maximum power block pressure and its power consumption remains constant with a value of 0.417 kW. As a result of those, the system energy efficiency increases from 31.97 % to 35.50 % and exergy efficiency rises from 51.85 % to 58.21 %.

5.2.3. Effects of the minimum power block temperature

The effects of the minimum power block temperature on the turbine power output, and compressor and pump power consumption are shown in Fig. 11, correspondingly the system energy and exergy efficiencies are given in Fig. 12. As the minimum temperature changes from 31.0 °C to 32.5 °C, the turbine work output decreases significantly from 130.98 kW to 120.80 kW, this is due to the fact that as the temperature increases, less liquid is produced in the vortex tube, which is diverted into the turbine. Accordingly, the main and electrical compressor work slightly increase from 8.18 kW to 8.59 kW and 0.13 kW to 0.59 kW, respectively. Therefore, the system energy and exergy efficiencies decrease from 35.5 % and 58.21 % to 35.41 % and 58.06 %, respectively.

5.2.4. Effects of the maximum power block temperature

The influences of the maximum power block temperature on the turbine power output, compressor and pump power consumption are indicated in Fig. 13, the system energy and exergy efficiencies are given in Fig. 14. As the maximum temperature rises from 300 °C to 800 °C, the power consumption of the pump, electrical and main compressors remain constant at 15.79 kW, 0.4179 kW and 8.43 kW respectively but the turbine power output increases from 74.53 kW to 155.39 kW due to the exergy growth of the inlet state. Correspondingly, the system energy efficiency increases from 21.54 % to 41.84 % and exergy efficiency enhance from 55.36 % to 60.80 %.

5.2.5. Effects of the mass flow rate split ratio

The effects of the split ratio, which is the ratio of the mass flow rate diverted to the power block to the total mass flow rate of the system, on the system power generation and consumption are given in Fig. 15, the system energy and exergy efficiencies for different split ratios are shown in Figs. 16 and 17, respectively. As the split ratio increases, there is more working fluid diverted to the main compressor, this leads to its high power consumption. As the split ratio rises from 0.1 to 0.7, the turbine power output increases from 122.88 kW to 130.46 kW owing to more working fluid through the turbine, the main compressor power consumption increases from 2.81 kW to 22.48 kW, while the pump and electrical compressor power consumption decrease from 20.30 kW and 0.53 kW to 4.51 kW and 0.11 kW due to the less working fluid diverted to the vortex tube. When the split ratio is 0.203, the system energy and exergy efficiencies reach the highest values of 35.56 % and 58.32 % respectively.

5.2.6. Combined effects

Similar to the conventional recompression cycle, the split ratio is one of the key operation parameters in the system. In order to investigate combined effects of the split ratio and power block operating parameters, four case studies are conducted. In the first and second cases, the

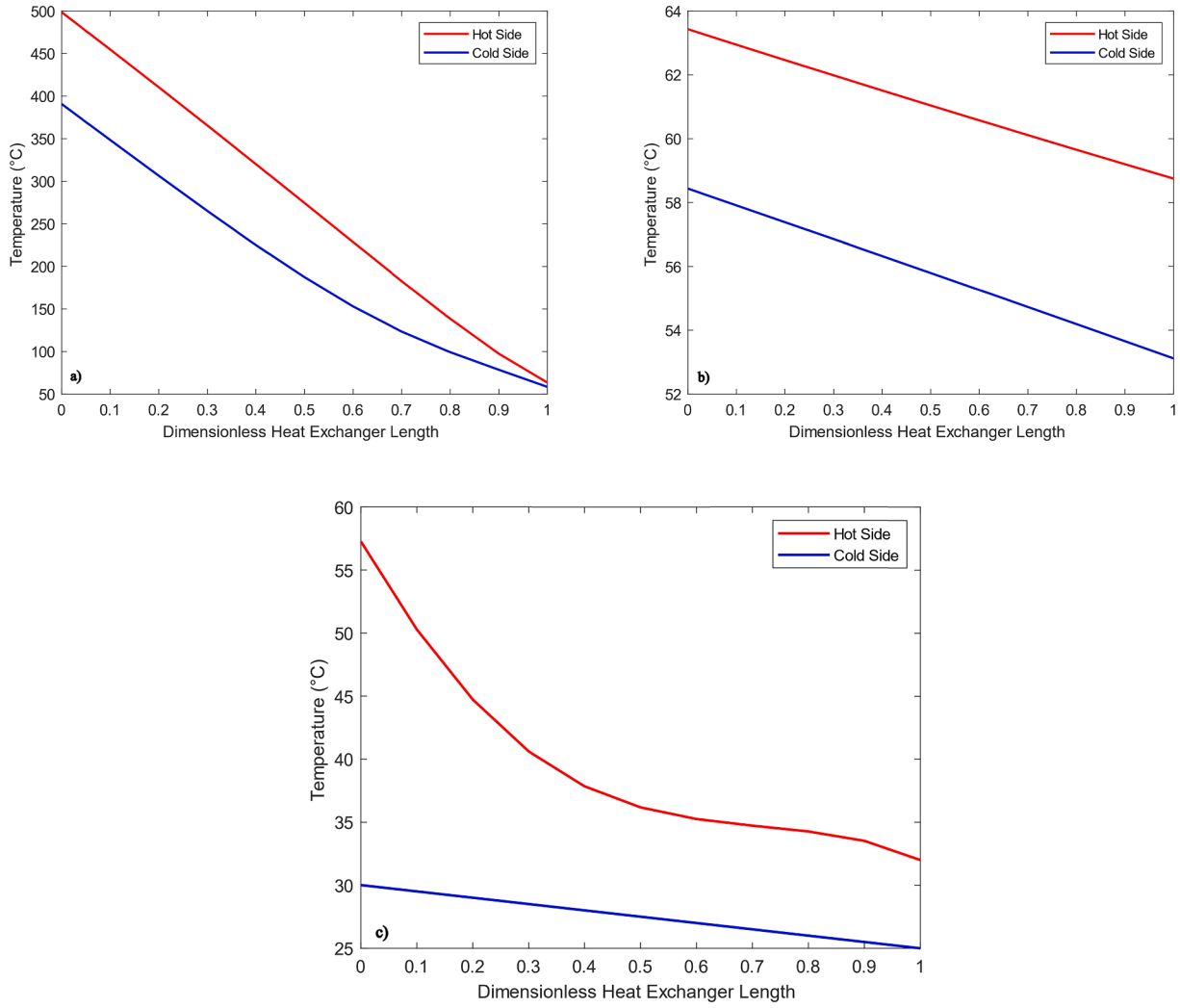

Fig. 6. Temperature distributions in the a) HTR b) LTR c) Air cooler.

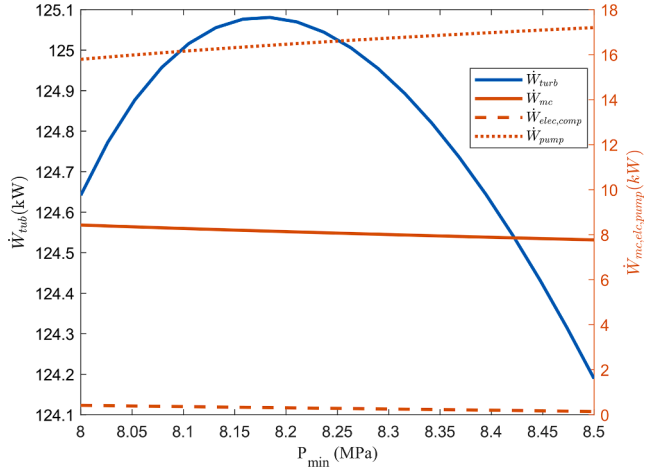

Fig. 7. Variations of turbine power output, main and electrical compressors, and pump power consumption with the minimum power block pressure.

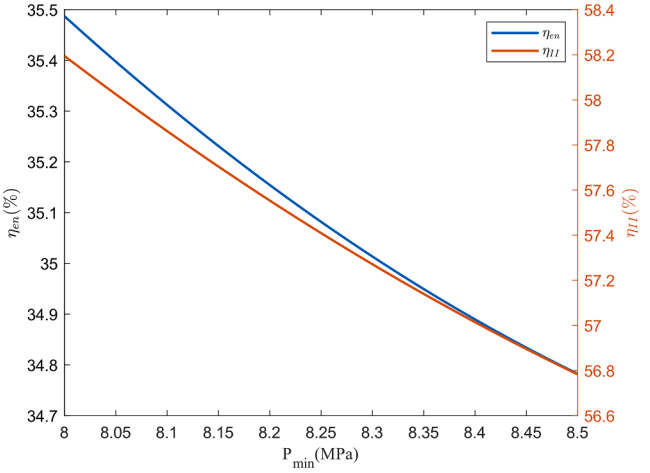

Fig. 8. Variations of energy and exergy efficiencies with the minimum power block pressure.

combined effects of the split ratio with the minimum and maximum power block pressures are investigated. In the third and fourth cases, the combined effects of the split ratio with the minimum and maximum power block temperatures are explored. The variations of the exergy efficiency with the split ratio, minimum and maximum pressures, minimum and maximum temperatures are presented in Figs. 17, 18, 19 and 20 respectively. At first, for the combined influence of the minimum power block pressure and split ratio, as the minimum pressure rises from

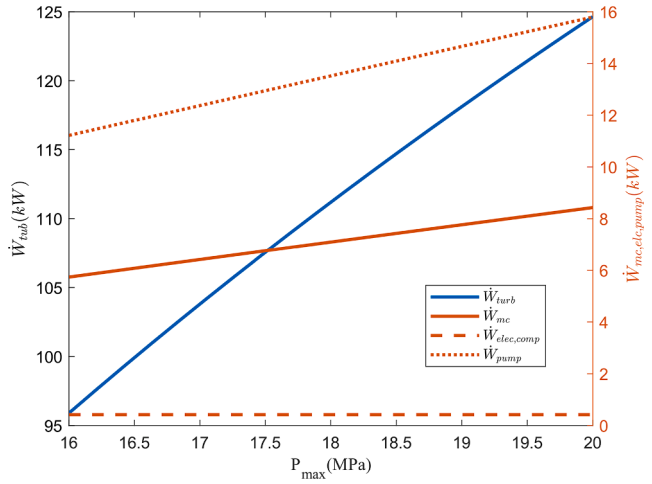

Fig. 9. Variations of turbine power output, main and electrical compressors and pump power consumption with the maximum power block pressure.

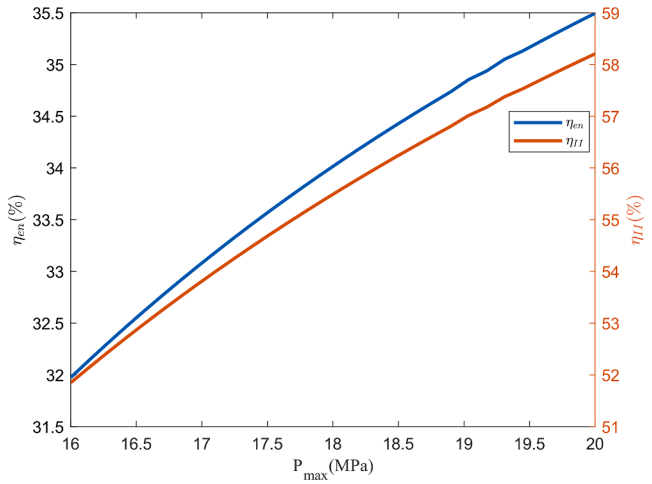

Fig. 10. Variations of energy and exergy efficiencies with the maximum power block pressure.

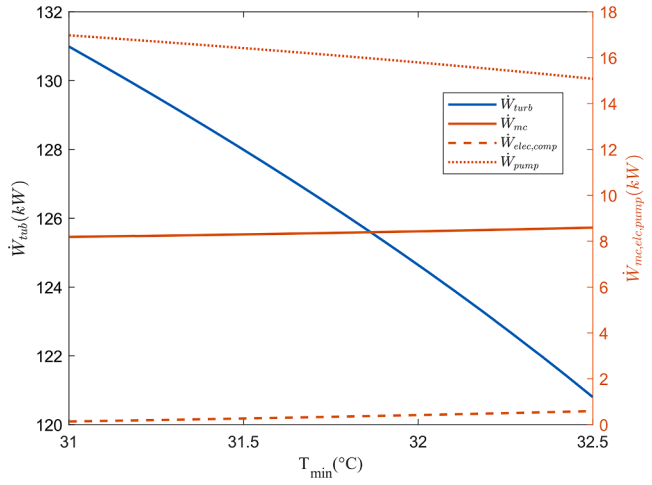

Fig. 11. Variations of turbine power output, and compressor and pump power consumption with the minimum power block temperature.

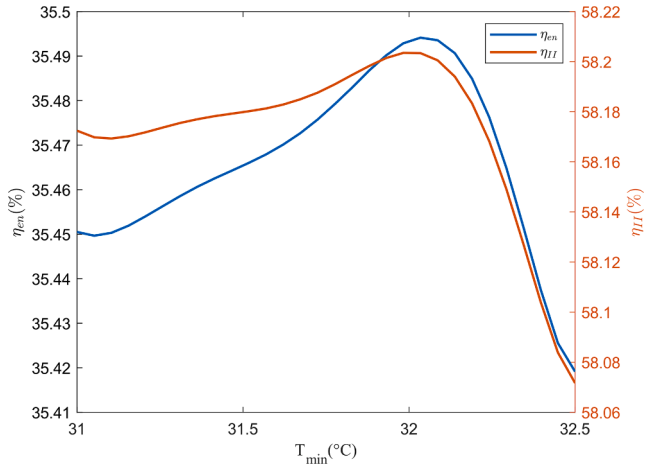

Fig. 12. Variations of energy and exergy efficiencies with the minimum power block temperature.

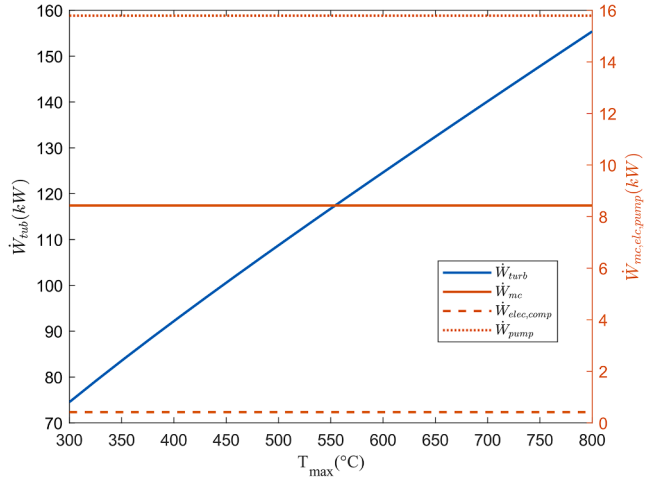

Fig. 13. Variations of turbine power output, and compressor and pump power consumption with the maximum power block temperature.

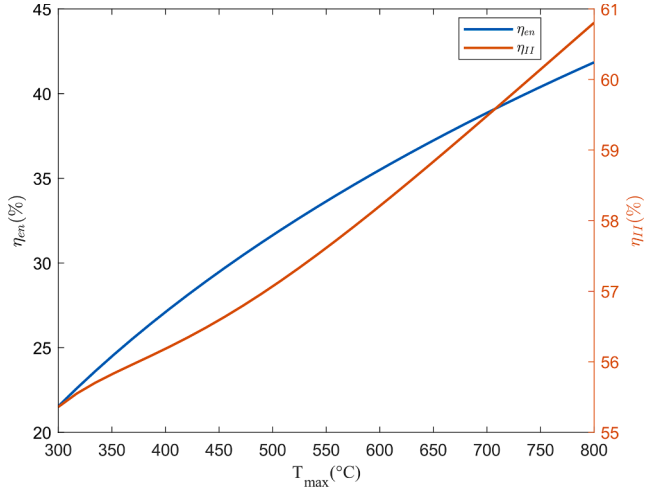

Fig. 14. Variations of energy and exergy efficiencies with the maximum power block temperature.

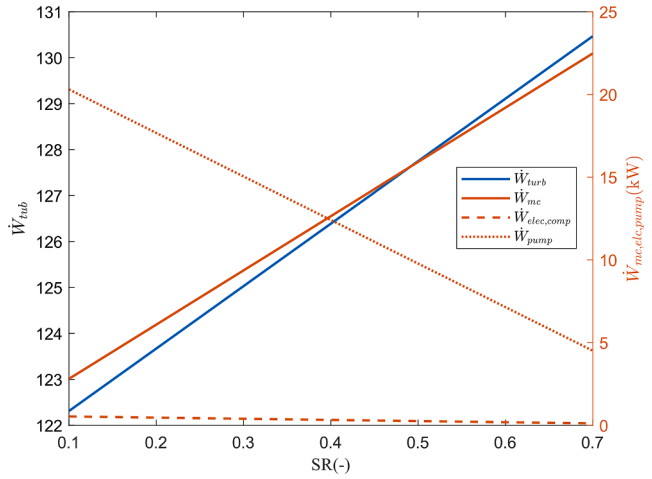

Fig. 15. Variations of turbine power output, compressor and pump power consumption with split ratio.

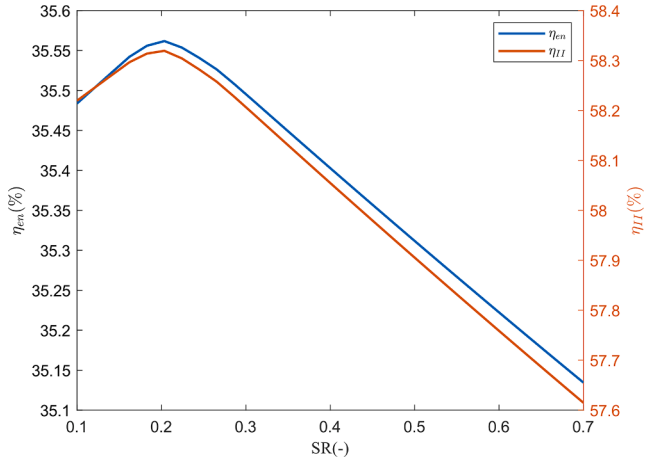

Fig. 16. Variations of energy and exergy efficiencies with split ratio.

8.0Mpa to 8.5Mpa and the split ratio increases from 0.1 to 0.7, the power consumption by the main compressor increases from 2.81 kW to 18.12 kW, the system exergy efficiency decreases from 58.22 % to 56.59 %. The turbine power output increases with the split ratio as more fluid enters the turbine, but decreases with the minimum pressure because the turbine expansion ratio is reduced. This contradicting relation between the minimum pressure and split ratio leads to the highest exergy efficiency of 58.32 % at the split ratio of 0.203 and the minimum pressure of 8.0 Mpa.

Similarly, as for the combined effect of the maximum power block pressure and split ratio, when the maximum pressure and split ratio increase from 16Mpa to 20Mpa and from 0.1 to 0.7, the turbine power output increases from 94.10 kW to 129.3 kW due to the increases in expansion pressure ratio and flow rate. At the same time, the main compressor work increases significantly from 1.91 kW to 19.67 kW, the system exergy efficiency varies from 51.73 % to 57.61 %. The system highest exergy efficiency of 58.32 % is achieved at the split ratio of 0.197 and the maximum pressure of 20Mpa in this case.

As the minimum power block temperature and split ratio increase from 31 °C to 32.6 °C and from 0.1 to 0.7, the power produced by the turbine slightly decreases from 129.73 kW to 127.65 kW owing to less amount of liquid is produced by the vortex tube, the main compressor work increases from 2.72 kW to 20.04 kW due to the increases in compressor mass flow rate and inlet temperature. As the minimum temperature increases, less amount of liquid is produced by the vortex tube. In this case, the system reaches the highest exergy efficiency of 58.33 % when the split ratio is 0.197 and the minimum temperature is 32.0 °C.

For the combined effect of the maximum power block temperature and split ratio, as the maximum temperature decreases from 800 °C to 400 °C and the split ratio increases from 0.1 to 0.7, the power production by the turbine changes from 161.20 kW to 90.48 kW, the system exergy efficiency reduces from 60.33 % to 55.89 % due to the decrease in exergy available at the turbine inlet state. In this case, the system reaches the highest exergy efficiency of 60.88 % when the split ratio is 0.203 and the maximum temperature is 800 °C.

5.3. Optimization

Changes of the maximum exergy efficiency and mean value of it in

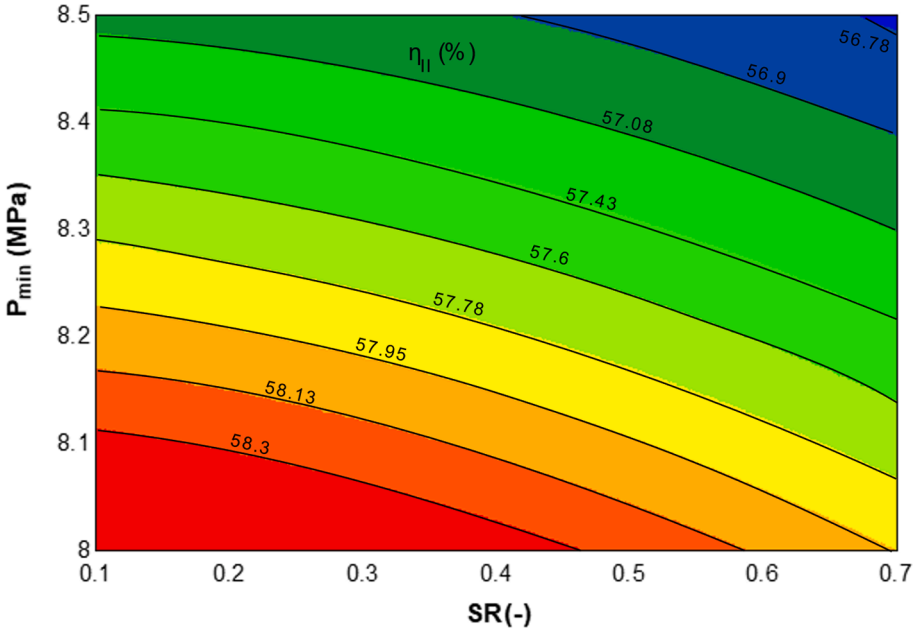

Fig. 17. Variation of the exergy efficiency with the minimum power block pressure and split ratio.

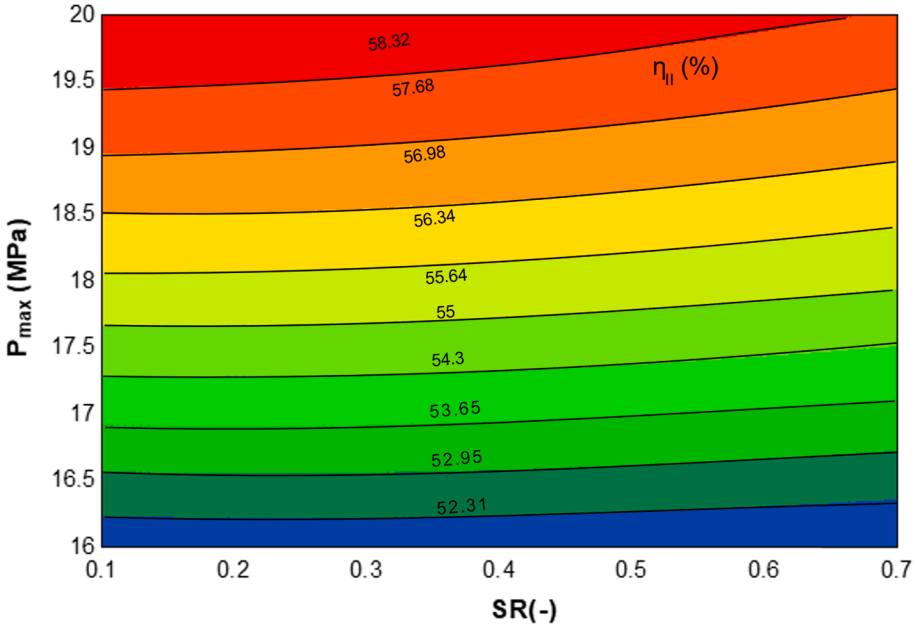

Fig. 18. Variation of the exergy efficiency with the maximum power block pressure and split ratio.

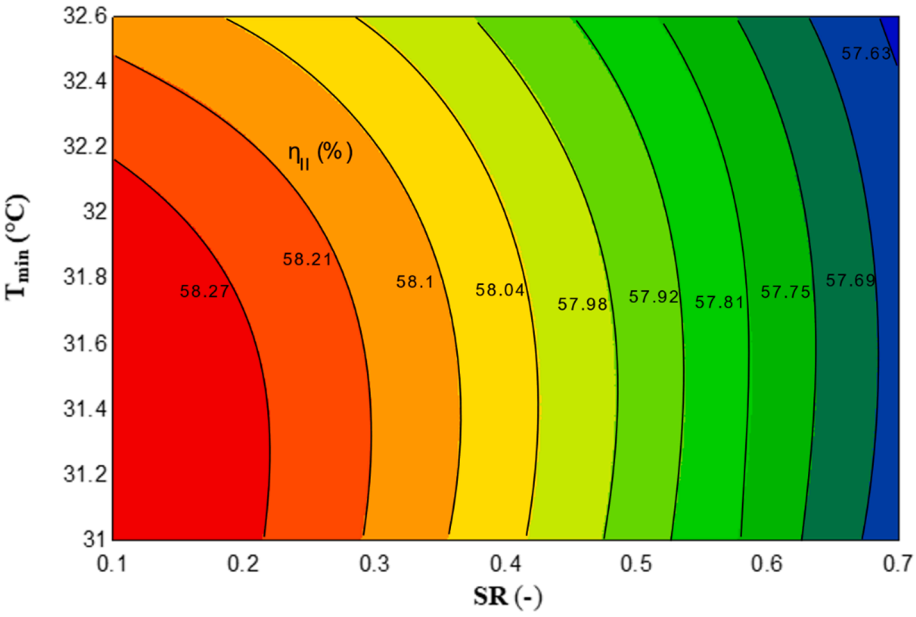

Fig. 19. Variation of the exergy efficiency with the minimum power block temperature and split ratio.

each generation are shown in Fig. 21. Optimization process is terminated in 117th generation because the average change in the objective function is too small, the maximum exergy efficiency is found when the minimum power block pressure is 8.01Mpa, the maximum pressure is 20Mpa, the minimum power block temperature is 32 °C, the maximum temperature is 800 °C, and the split ratio is 0.201. The system maximum net power output is reached with a value of 129.76 kW, correspondingly the system maximum energy and exergy efficiencies are 41.9 % and 60.89 % respectively. All performance parameters of the optimal operation state are given in Table 7.

6. Conclusions

A novel self-condensing sCO_2 recompression system with vortex tube is presented in this paper. The system performance is investigated from the first and second laws of thermodynamics point of view, and parametric analyses are carried out in order to clarify influences of key design and operation parameters on the system performance. Following conclusions can be drawn based on results of this study:

- In a base case scenario with 100 kW power output, the energy and exergy efficiencies of the self-condensing sCO_2 recompression system reach 35.5 % and 58.21 % respectively, which are higher than those of the traditional sCO_2 recuperation system.
- The recuperator is the largest contributor to the system irreversibility with a value of 45.12 kW due to the high heat duty, while the electrical compressor is the smallest contributor with a value of 0.079 kW owing to the low pressure ratio and mass flow rate.
- The minimum power block pressure affects the vortex tube and turbine performance in the opposite way. As the minimum pressure

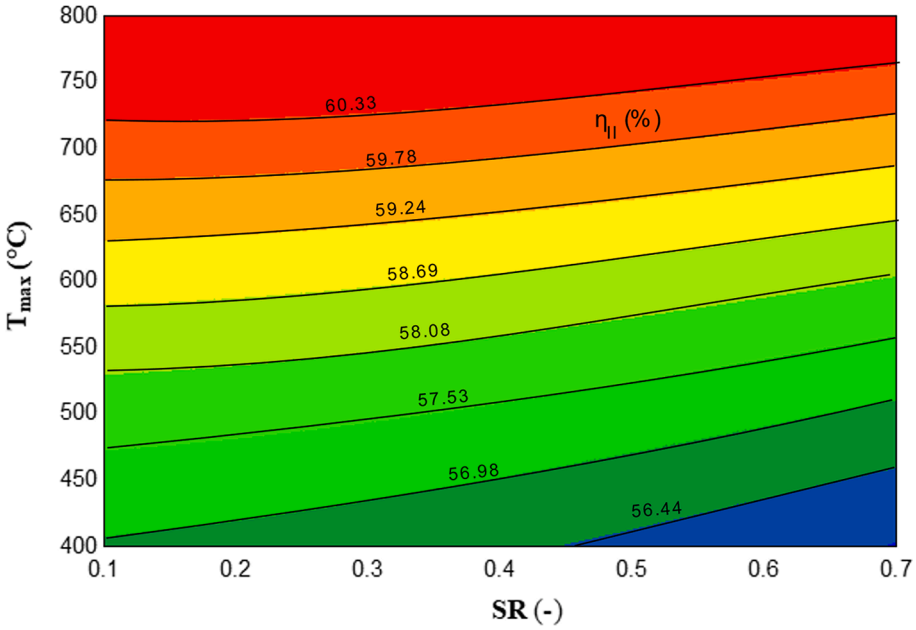

Fig. 20. Variation of the exergy efficiency with the maximum power block temperature and split ratio.

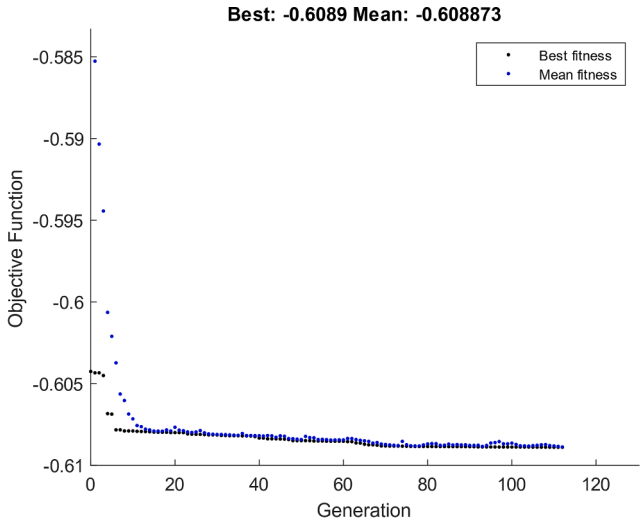

Fig. 21. Iterative process of exergy efficiency.

Table 7
Optimal operation parameters for self-condensing sCO_2 recompression system.

Operation Variable	Value	Performance Parameter	Value
Minimum Power Block Pressure P_{min} (Mpa)	8.01	$\dot{W}_{turb}$ (kW)	153.95
Maximum Power Block Pressure P_{max} (Mpa)	20	$\dot{W}_{comp}$ (kW)	5.64
Maximum Power Block Temperature T_{max} (°C)	799	w_{comp} (kJ/kg)	4.85
Minimum Power Block Temperature T_{min} (°C)	32.0	$\dot{W}_{elec,comp}$ (kW)	0.4770
Split Ratio	0.201	$w_{elec,comp}$ (kJ/kg)	0.410
		$\dot{W}_{pump}$ (kW)	18.02
		w_{pump}(kJ/kg)	15.50
		$\dot{W}_{net}$ (kW)	129.80
		Q_{gh} (kW)	309.8
		η_{en} (%)	41.9
		η_{II} (%)	60.89

increases from 8.0Mpa to 8.5Mpa, liquid generated rate in the vortex tube increases from 0.7424 kg/s to 0.8087 kg/s, but the turbine expansion ratio decreases from 2.5 to 2.35, the system energy and exergy efficiencies decrease from 35.50 % and 58.21 % to 34.77 % and 56.77 %, respectively.

- The minimum power block temperature has the influences on the turbine and compressor performance. As the minimum temperature rises from 31 °C to 32.5 °C, the turbine power output drops from 130.98 kW to 120.8 kW, the main and electrical compressor work increase slightly from 8.18 kW to 8.59 kW and 0.13 kW to 0.59 kW, respectively.
- The mass flow rate split ratio has a significant effect on the system performance. As the split ratio rises from 0.1 to 0.7, the main compressor work increases from 2.81 kW to 22.48 kW, the pump power consumption decreases from 20.30 kW to 4.51 kW. The system achieves the highest energy and exergy efficiencies of 35.56 % and 58.32 % respectively as the split ratio is 0.197.
- The system energy and exergy efficiencies reach the maximum values of 41.9 % and 60.89 % respectively when the minimum power block pressure is 8.01Mpa, the maximum power block pressure is 20Mpa, the minimum power block temperature is 32 °C, the maximum power block temperature is 800 °C and the split ratio is 0.201.

The proposed system can be a promising solution for achieving self-condensation and high efficiency without low temperature heat sink. The system can be powered by various heat sources, such as industrial waste heat and solar energy. For the future work, the potential cogeneration configuration will be investigated from energy and economical aspects.

CRediT authorship contribution statement

Tugberk Hakan Cetin: Conceptualization, Methodology, Software, Visualization, Data curation. **Jie Zhu:** Methodology, Conceptualization, Supervision.

Declaration of Competing Interest

The authors declare that they have no known competing financial

interests or personal relationships that could have appeared to influence the work reported in this paper.

Data availability

Data will be made available on request.

Acknowledgment

The financial support from TUBITAK under 2213/A-Overseas Graduate Scholarship Program is gratefully acknowledged by the authors.

References

[1] Cozzi L. International EA, Gould T (International EA). World Energy Outlook 2021; 2021:1–386.
[2] Goldstein B, Gounaridis D, Newell JP. The carbon footprint of household energy use in the United States. Proc Natl Acad Sci U S A 2020;117(32):19122–30.
[3] Guo J-Q, Li M-J, He Y-L, Jiang T, Ma T, Xu J-L, et al. A systematic review of supercritical carbon dioxide(S-CO2) power cycle for energy industries: technologies, key issues, and potential prospects. Energy Convers Manag 2022;258: 115437. https://doi.org/10.1016/j.enconman.2022.115437.
[4] Alenezi A, Vesely L, Kapat J. Exergoeconomic analysis of hybrid sCO$_2$ Brayton power cycle. Energy 2022;247:123436. https://doi.org/10.1016/j.energy.2022.123436.
[5] Thanganadar D, Fornarelli F, Camporeale S, Asfand F, Patchigolla K. Off-design and annual performance analysis of supercritical carbon dioxide cycle with thermal storage for CSP application. Appl Energy 2021;282:116200. https://doi.org/10.1016/j.apenergy.2020.116200.
[6] Rogalev N, Rogalev A, Kindra V, Komarov I, Zlyvko O. Structural and Parametric Optimization of S-CO$_2$ Nuclear Power Plants. Entropy 2021;23:1079. https://doi.org/10.3390/E23081079.
[7] Chen Z, Wang Y, Zhang X. Energy and exergy analyses of S-CO$_2$ coal-fired power plant with reheating processes. Energy 2020;211:118651. https://doi.org/10.1016/j.energy.2020.118651.
[8] Alfani D, Binotti M, Macchi E, Silva P, Astolfi M. sCO2 power plants for waste heat recovery: design optimization and part-load operation strategies. Appl Therm Eng 2021;195:117013. https://doi.org/10.1016/j.applthermaleng.2021.117013.
[9] Li B, Wang S-S, Xu Y, Song L. Study on the off-design performance of supercritical carbon dioxide power cycle for waste heat recovery of gas turbine. Energy Convers Manag 2021;233:113890. https://doi.org/10.1016/j.enconman.2021.113890.
[10] Chen R, Romero M, González-Aguilar J, Rovense F, Rao Z, Liao S. Design and off-design performance comparison of supercritical carbon dioxide Brayton cycles for particle-based high temperature concentrating solar power plants. Energy Convers Manag 2021;232:113870. https://doi.org/10.1016/j.enconman.2021.113870.
[11] Gao L, Cao T, Hwang Y, Radermacher R. Graph-based configuration optimization for S-CO$_2$ power generation systems. Energy Convers Manag 2021;244:114448. https://doi.org/10.1016/j.enconman.2021.114448.
[12] Gao L, Cao T, Hwang Y, Radermacher R. Robustness analysis in supercritical CO$_2$ power generation system configuration optimization. Energy 2022;242:122956. https://doi.org/10.1016/j.energy.2021.122956.
[13] Shu G, Shi L, Tian H, Li X, Huang G, Chang L. An improved CO$_2$-based transcritical Rankine cycle (CTRC) used for engine waste heat recovery. Appl Energy 2016;176: 171–82. https://doi.org/10.1016/J.APENERGY.2016.05.053.
[14] Angelino G. Carbon dioxide condensation cycles for power production 1968.
[15] Xia G, Sun Q, Cao X, Wang J, Yu Y, Wang L. Thermodynamic analysis and optimization of a solar-powered transcritical CO$_2$ (carbon dioxide) power cycle for reverse osmosis desalination based on the recovery of cryogenic energy of LNG (liquefied natural gas). Energy 2014;66:643–53. https://doi.org/10.1016/J.ENERGY.2013.12.029.
[16] Angelino G, Invernizzi CM. Carbon dioxide power cycles using liquid natural gas as heat sink. Appl Therm Eng 2009;29(14-15):2935–41.
[17] Yang P, Yuan M, Liu Z, Xie N, Liu Y, Yang S. Multi- objective optimization and life cycle assessment of a cascade system integrating LiBr/H$_2$O absorption refrigeration with transcritical CO$_2$ power cycle. Energy Convers Manag 2021;244:114453. https://doi.org/10.1016/j.enconman.2021.114453.
[18] Muhammad HA, Cho J, Cho J, Choi B, Roh C, Ishfaq HA, et al. Performance improvement of supercritical carbon dioxide power cycle at elevated heat sink temperatures. Energy 2022;239:122216. https://doi.org/10.1016/j.energy.2021.122216.
[19] Luo X, Chen P, Liang Y, Chen J, Yang Z, Wang C, et al. Thermodynamic analysis and evaluation of a novel trans-critical CO$_2$ power system incorporating partial condensation, sub-cooling, and recompression. Energy Convers Manag 2022;259: 115580. https://doi.org/10.1016/j.enconman.2022.115580.
[20] Pan L, Li B, Shi W, Wei X. Optimization of the self-condensing CO$_2$ transcritical power cycle using solar thermal energy. Appl Energy 2019;253:113608. https://doi.org/10.1016/j.apenergy.2019.113608.
[21] Pan L, Shi W, Wei X, Li T, Li Bo. Experimental verification of the self-condensing CO$_2$ transcritical power cycle. Energy 2020;198:117335. https://doi.org/10.1016/j.energy.2020.117335.
[22] Liu Z, Liu Z, Cao X, Li H, Yang X. Self-condensing transcritical CO2 cogeneration system with extraction turbine and ejector refrigeration cycle: a techno-economic assessment study. Energy 2020;208:118391. https://doi.org/10.1016/j.energy.2020.118391.
[23] Zhao P, Xu W, Gou F, Fan G, Wang J. Performance analysis of a self-condensation compressed carbon dioxide energy storage system with vortex tube. J Energy Storage 2021;41:102995. https://doi.org/10.1016/j.est.2021.102995.
[24] Liu Y, Sun Y, Tang D. Analysis of a CO$_2$ transcritical refrigeration cycle with a vortex tube expansion. Sustain 2019;11:2021. https://doi.org/10.3390/SU11072021.
[25] Qyyum MA, Wei F, Hussain A, Noon AA, Lee M. An innovative vortex-tube turbo-expander refrigeration cycle for performance enhancement of nitrogen-based natural-gas liquefaction process. Appl Therm Eng 2018;144:117–25. https://doi.org/10.1016/J.APPLTHERMALENG.2018.08.023.
[26] Maestre-Cambronel D, Guzmán Barros J, Gonzalez-Quiroga A, Bula A, Duarte-Forero J. Thermoeconomic analysis of improved exhaust waste heat recovery system for natural gas engine based on Vortex Tube heat booster and supercritical CO$_2$ Brayton cycle. Sustain Energy Technol Assessments 2021;47:101355. https://doi.org/10.1016/j.seta.2021.101355.
[27] Wang J, Liao G, Zuo Q, Guo Y, Zhao P, Dai Y. Economic analysis, and multiobjective optimization of a novel transcritical CO$_2$ Rankine Cycle with a vortex tube. J Energy Eng 2022;148(1). https://doi.org/10.1061/(ASCE)EY.1943-7897.0000810.
[28] Song Y, Wang J, Dai Y, Zhou E. Thermodynamic analysis of a transcritical CO$_2$ power cycle driven by solar energy with liquified natural gas as its heat sink. Appl Energy 2012;92:194–203. https://doi.org/10.1016/J.APENERGY.2011.10.021.
[29] Cengel YA, Boles MA, Kanoglu M. Thermodynamics : an engineering approach 2019.
[30] Balli O, Aygun H, Turan O. Enhanced dynamic exergy analysis of a micro-jet (μ-jet) engine at various modes. Energy 2022;239:121911. https://doi.org/10.1016/j.energy.2021.121911.
[31] Wark 1927- K. Advanced thermodynamics for engineers. New York : McGraw-Hill, [1995] ©1995; n.d.
[32] Sarkar J. Cycle parameter optimization of vortex tube expansion transcritical CO2 system. Int J Therm Sci 2009;48(9):1823–8.
[33] Maurer T. Patent DE 197 48 083 A1. Entspannungseinrichtung 1999.
[34] Kotas TJ. The exergy method of thermal plant analysis. Paragon Publishing; 2012.
[35] Arora J. Introduction to optimum design. Elsevier; 2004.
[36] Aygun H, Turan O. Application of genetic algorithm in exergy and sustainability: a case of aero-gas turbine engine at cruise phase. Energy 2022;238:121644. https://doi.org/10.1016/j.energy.2021.121644.
[37] Jafarzad A, Asgari N, Ranjbar F, Mohammadkhani F. Thermodynamic assessment and optimization of the influences of the steam-assisted turbocharging and organic Rankine cycle on the overall performance of a diesel engine-based cogeneration integrated with a reverse osmosis desalination unit. Sustain Energy Technol Assessments 2021;46:101175. https://doi.org/10.1016/j.seta.2021.101175.
[38] Bell IH, Wronski J, Quoilin S, Lemort V. Pure and pseudo-pure fluid thermophysical property evaluation and the open-source thermophysical property library coolprop. Ind Eng Chem Res 2014;53:2498–508. https://doi.org/10.1021/IE4033999/SUPPL_FILE/IE4033999_SI_002.ZIP.
[39] Abbasi HR, Pourrahmani H. Multi-objective optimization and exergoeconomic analysis of a continuous solar-driven system with PCM for power, cooling and freshwater production. Energy Convers Manag 2020;211:112761. https://doi.org/10.1016/j.enconman.2020.112761.
[40] Pan M, Bian X, Zhu Y, Liang Y, Lu F, Xiao G. Thermodynamic analysis of a combined supercritical CO$_2$ and ejector expansion refrigeration cycle for engine waste heat recovery. Energy Convers Manag 2020;224:113373. https://doi.org/10.1016/j.enconman.2020.113373.
[41] Liu Y, Sun Y, Wang D. Research on carbon dioxide transcritical refrigeration cycle with vortex tube. IOP Conf Ser Earth Environ Sci 2019;267(2):022010. https://doi.org/10.1088/1755-1315/267/2/022010.
[42] Wang L, Pan L-M, Wang J, Chen D, Huang Y, Hu L. Investigation on the temperature sensitivity of the S-CO$_2$ Brayton cycle efficiency. Energy 2019;178: 739–50.